ACS APPLIED MATERIALS & INTERFACES

Research Article

www.acsami.org

Inkjet-Printed Gold Electrodes on Paper: Characterization and Functionalization

Anni Määttänen,*[,†] Petri Ihalainen,[†] Petri Pulkkinen,[‡] Shaoxia Wang,[§] Heikki Tenhu,[‡] and Jouko Peltonen[†]

[†]Center of Excellence for Functional Materials, Laboratory of Physical Chemistry, [§]Center of Excellence for Functional Materials, Laboratory of Paper Coating and Converting, Åbo Akademi University, Porthaninkatu 3, FI-20500 Turku, Finland

[‡]Center of Excellence for Functional Materials, Laboratory of Polymer Chemistry, University of Helsinki, P.O. Box 55, FI-00014 Helsinki, Finland

Supporting Information

ABSTRACT: Gold nanoparticles were synthesized and inkjet-printed on a paper substrate and IR-sintered to produce conductive electrodes. The electrodes were further functionalised by using self-assembled octadecanethiol monolayers (SAMs). The effect of sintering, print quality, and SAM formation were examined by topographical, chemical and electrical methods. With optimised printing parameters, a volume resistivity of ~1.6 $\times 10^{-7}$ Ω m was attained by a single print layer.

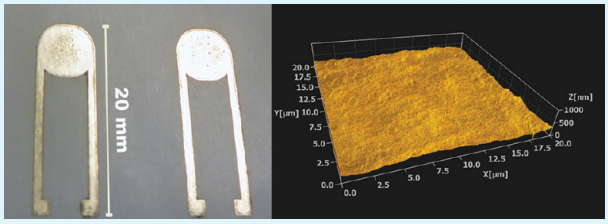

KEYWORDS: *printed electronics, gold nanoparticles, paper, inkjet-printing, self-assembled monolayer*

1. INTRODUCTION

High-resolution printing of metal-based nanoparticle (NP) inks enable cost-effective and simple fabrication of conductive structures.[1−13] Factors that control the morphology and conductivity of the printed patterns have been extensively studied in order to optimise the printing and curing conditions.[14−20] Silver (Ag) NPs have been readily used in printed electronics, including transistors and solar cells, on various print substrates.[14−16,21−24] Despite the relatively high conductivity achieved with AgNPs, it is not a suitable electrode material for all applications due to its reactivity. Oxidation of silver electrodes has been shown to cause problems in polymer solar cells.[25] In addition, silver is prone to diffuse into the active material (e.g. the semiconductor and dielectric layer in organic thin film transistors) causing short-circuits.[26,27] Gold, on the other hand, is chemically inert and has excellent resistance to oxidation and acids. The good biocompatibility[28] and high affinity of alkanethiols for gold nanoparticles (AuNPs)[29] promote their applicability in various fields e.g. nano-medicine[30−33] and printed electronics.[34−36] The low sintering temperatures of AuNPs compared to the bulk gold (1063 °C)[37] enable reduced processing temperatures and the use of various substrates. Conductive gold structures have been fabricated by inkjet printing on glass,[38−41] silicone,[42] plastic[6,43] and paper substrates.[27,44] Various methods have been utilised for the sintering of printed AuNP patterns, including hot plate, oven, infrared (IR) sintering, and laser.

In the present study, a high-yield, low-material-consumption fabrication of printed Au electrodes on paper is demonstrated. IR sintering allowed a rapid annealing of printed AuNP layers, resulting in a low-resistance film without the degradation of the substrate. The print parameters were optimised in order to obtain a smooth electrode surface for the self-assembly process. Succesfull SAM formation was confirmed by chemical analysis and electrostatic experiments.

2. MATERIALS AND METHODS

2.1. Synthesis and Characterization of the Gold Nanoparticles. The chemicals were purchased from Sigma-Aldrich and used without further purification. Dodecanethiol-protected AuNPs were synthesised following the procedure reported by Hostetler et al.[34] $HAuCl_4 \cdot H_2O$ (1.75 mmol) in 25 mL of deionized water was added into 40 mL of vigorously stirred toluene with 4.38 mmol of tetraoctylammonium bromide (TOAB). After the gold salt was fully transferred into the organic phase, the water phase was discarded. 0.44 mmol of dodecanethiol was added and the mixture was stirred for 10 min. The reaction mixture was vigorously stirred and 17.5 mmol of $NaBH_4$ in 25 mL of water was added in a single fast injection. The resulting dark solution was stirred for 3 h. The organic phase was collected and evaporated. The black product was dispersed in ethanol and filtered. The residue was washed with copious amounts of ethanol and acetone. The final black powder was dried in a vacuum.

The size and shape of the synthesized nanoparticles were examined by transmission electron microscopy using a Hitachi S4800 field-emission scanning electron microscope (FESEM) (Supporting Information 1). TEM samples were prepared by applying a droplet of 1 mg/mL toluene solution of the nanoparticles on a holey carbon film TEM grid (Cu mesh). A relatively narrow size distribution, roughly in the size range of 3.0 ± 1.8 nm, was obtained by an image analysis of over 800 particles (using Scanning Probe Image Processor software (SPIP, Image Metrology, Denmark)). Thermogravimetric

Received: November 17, 2011
Accepted: January 10, 2012
Published: January 10, 2012

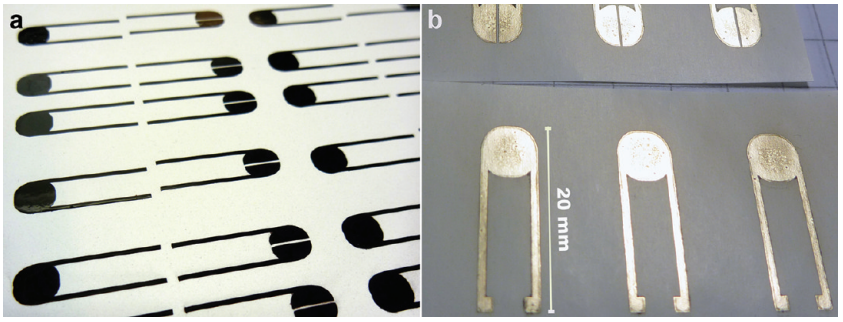

Figure 1. Photographs of the (a) unsintered and (b) IR-sintered inkjet-printed Au electrodes on paper.

analysis (TGA) was carried out under a flowing nitrogen atmosphere using Mettler Toledo TGA850 equipment with STARe software. Pyrolysis of the dodecanethiol occurred at around 175 − 250°C (Supporting Information 2). This is consistent with results published by Huang et al.[12] According to TGA, the AuNPs contained 16.5 wt % volatile components.

2.2. Substrates. A pigment (kaolin) coated paper developed for printed functionality was used as a print substrate.[21,45,46] The thickness and grammage of the paper substrate was 130 ± 30 μm and 126 g/m^2, respectively. Evaporated gold on mica was used as a reference substrate in the contact angle and surface potential measurements.

2.3. Inkjet Printing. The AuNPs (15 wt %) were dispersed in xylene (Sigma-Aldrich). Inkjet printing of the AuNP ink was performed with a Dimatix Materials Printer (DMP-2800, FUJIFILM Dimatix, Inc. Santa Clara, USA). The printing was done in ambient conditions using a single nozzle, 10 pL drop volume, 27 ± 3 V firing voltage and a custom waveform to ensure optimal droplet formation. The print pattern was designed with Microsoft ® Paint (Version 5.1) software to allow simultaneous printing of gold electrodes with varying print amount by using different drop spacing (DS 20−45 μm), i.e., distance between two adjacent jetted droplets.

Sintering of the printed gold patterns was carried out using an IR drier (IRT systems, Hedson Technologies AB, Sweden) consisting of three lamps and a fan. The samples were cured until the colour changed from blackish to golden yellow after approximately 5 − 15 s depending on the pattern and drop spacing. The distance between the sample and the lamp was approximately 20 cm. The IR-dried samples are from now on referred to as IR-sintered. In addition, the samples that were left to dry in ambient air are referred to as air-dried.

2.4. Thiolation of Gold Electrodes. Self-assembled monolayer (SAM) experiments were conducted using 1-octadecanethiol (ODT, Fluka Chemika). To obtain reproducible gold surfaces for SAM formation, gold surfaces are typically pretreated by, for example, an exposure to UV irradiation or oxygen plasma followed by an immersion in ethanol.[47] As a pretreatment, just before the thiolation, the IR-sintered electrode surfaces were cleaned with plasma (air) flow (PDC-326, Harrick) for 2 min, rinsed with acetone and absolute ethanol, and dried with nitrogen gas. Samples treated in this way are referred to as plasma-cleaned. An SAM was formed by exposing the electrode surface to ethanol solution of ODT (5 mM, in liquid cell) for 60 min at room temperature in the dark. After thiolation, the substrates were removed from the solution and rinsed immediately with absolute ethanol and dried with nitrogen gas. These samples are referred to as thiolated.

2.5. Topographical and Phase Imaging. An NTEGRA Prima (NT-MDT, Russia) atomic force microscope (AFM) with Nova software (v 1.1.0.1851, NT-MDT, Russia) was used to analyse the topography of the samples in intermittent-contact mode. The images (1024 × 1024 pixels) were recorded in ambient conditions (RH = 23 ± 3%, T = 26 ± 2°C) using high resolution silicon cantilevers (Model: NSG10, NT-MDT, Russia), a scan speed of 0.2−0.5 Hz and a damping ratio of 0.6−0.7 Hz. The AFM images were processed and analysed with SPIP software.

2.6. Surface Potential Imaging. In surface potential (SP) imaging a map of the electrostatic potential on the sample surface is created. The procedure is a nulling technique as the tip travels above the sample surface in LiftMode. Whenever a potential difference between the tip and the sample occurs, a force is experienced by the tip and the cantilever. The force is nullified by varying the voltage of the tip so that the tip is at the same potential as the region of the sample surface underneath it. The voltage applied to the tip during mapping is plotted versus the in-plane coordinates, creating a three-dimensional surface potential image.[48]

The SP imaging was carried out with a Nanoscope V AFM (MultimodeTM series, Digital Instruments, Veeco Metrology Group, Santa Barbara, CA). The microscope was placed on an active vibration isolation table (MOD-1M, JRS Scientific Instruments, Switzerland) standing on a stone table to eliminate external vibrational noise. The samples were taped on metallic sample pucks by double sided Scotch tape. Conductive silver paint (ELECTROLUBE, HK Wentworth Ltd, UK) was used to connect the printed Au patterns with the grounded sample pucks to eliminate charging of the samples. Platinum/iridium coated silicon SCM-PIT cantilever (Veeco Instruments SAS, Dourdan CEDEX, France) was used in the measurements. The SP images (512 × 512 pixels) were measured at a lift height of 20 nm in ambient conditions (RH = 35 ± 5% and T = 25 ± 3°C) with a damping ratio of 0.7−0.8. Acquisition of the SP data was carried out line-by-line with the surface topography imaging in a two-pass measurement mode. For each line, the sample topography was recorded in the first pass using TappingMode and the SP data was obtained during the second pass without applying a voltage to the sample.

2.7. Contact Angle Measurements. Contact angle measurements were made using a CAM 200 contact angle goniometer (KSV Instruments Ltd). Contact angles of water (Millipore) were calculated as a function of time using the software supplied with the instrument, which utilises both a circular and a Laplace fit to the projected drop curvature. The used drop size was 4.0 ± 1 μL.

2.8. X-ray Photoelectron Spectroscopy. X-ray photoelectron spectroscopy (XPS) spectra were obtained with a PHI Quantum 2000 scanning spectrometer, using monochromatic Al KR (1486.6 eV) excitation and charge neutralisation by using electron filament and an electron gun. The photoelectrons were collected at 45° in relation to the sample surface with a hemispherical analyser. The analysing depth was approximately 5−10 nm. The pass energy was 117.4 and 23.5 eV for low and high resolution, respectively. The measurements were carried out on three different spots for each sample. An acquisition time of 10 min was used for both the survey and high-resolution spectra. A Gaussian curve-fitting program (MultiPak v6.1A, Physical Electronics) was used to deconvolute the C1s and S2p signals.

2.9. Electrical Resistance Measurements. Resistance measurements were done with a four-point measurement setup using a Keithley 2100 Digital Multimeter (Keithley Instruments Inc., Cleveland, USA). The electrical resistivity (ρ) of the printed and sintered Au-lines was calculated using the following formula: $\rho = R(Wd/L)$, where R is the electrical resistance, W is the width, d is the height and L is the length of the printed line.

A HEPES-EDTA aqueous solution (10 mM HEPES (Sigma), 150 mM NaCl (Fluka), 1 mM EDTA (Sigma), pH 7.4) was used as an electrolyte solution in the electrochemical measurements.

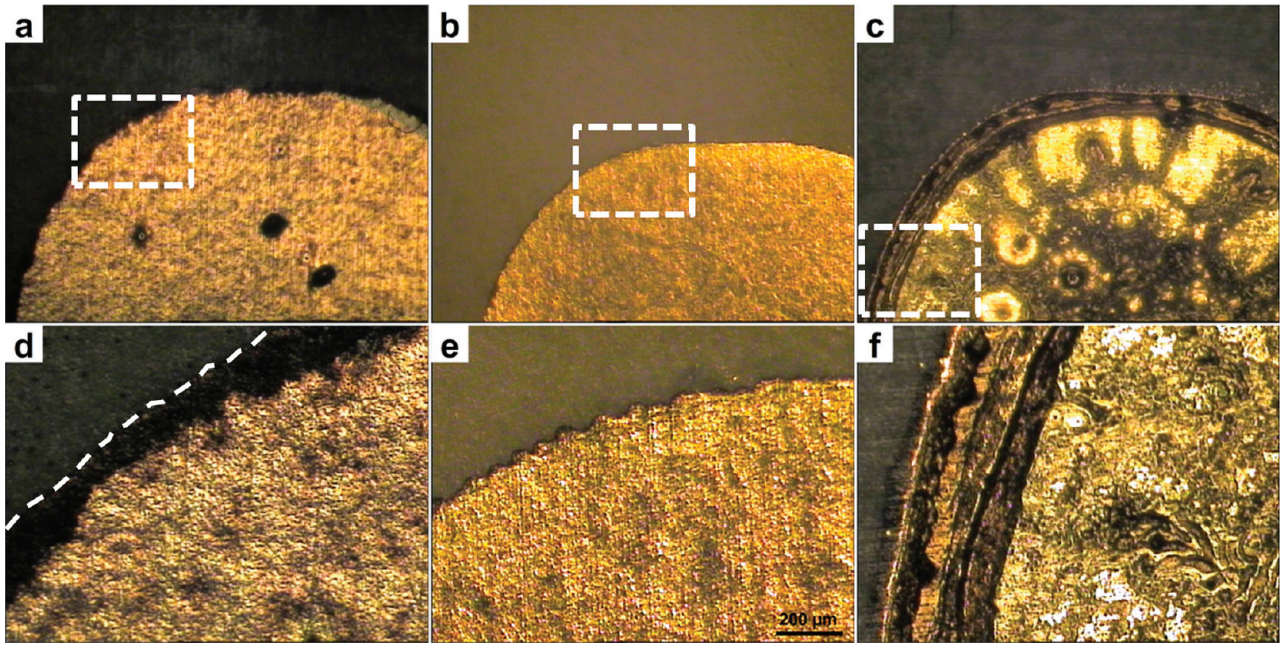

Figure 2. Optical micrographs of the IR-sintered Au electrodes printed with a DS of (a) 40, (b) 30, and (c) 20 μm. The rectangles in a–c indicate the locations of the higher magnification micrographs (d, e). The dashed line in d highlights the edge of the print.

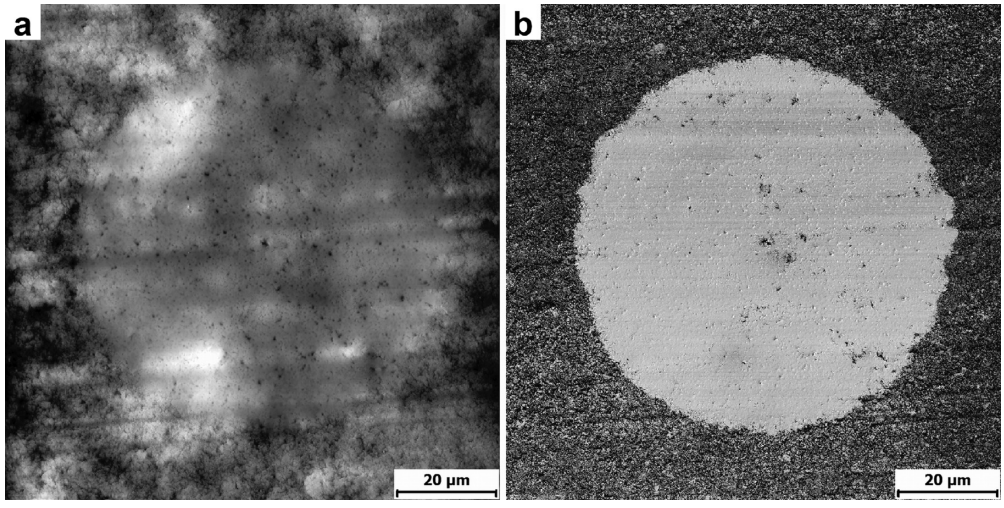

Figure 3. (a) AFM topographical and (b) phase image of an unsintered inkjet-droplet of Au ink printed on paper. The z-scales are (a) 1 μm and (b) 100°.

2.10. Optical Microscope Micrographs. Optical micrographs (OM) were captured with an optical microscope (OPTEM 125, Qioptiq LINOS, Inc., USA) using a nominal magnification of 0.52 and 2.0×.

3. RESULTS

3.1. Visual Characterization of the AuNP Structures. Figure 1 shows photographs of the inkjet-printed Au electrode structures (a) before and (b) after IR sintering. The unsintered Au electrodes were blackish and non-conductive even if they were left to dry in ambient air for several weeks. IR sintering changed the colour of the electrodes gradually to golden starting from the center and proceeding towards the edges of the print. This was most probably because of a higher thickness of the printed AuNPs in the center of the printed pattern. After IR sintering for 10–15 s, the color change was completed and the printed patterns had become conductive.

Optical microscope micrographs of IR-sintered electrode structures printed with different DS-values are shown in Figure 2. The homogeneity of reflection and color varied depending on the used DS value. For low amounts of printed material (DS 35–45 μm) the surfaces were less reflective (Figure 2a, d). In addition the edges of the print remained dark (Figure 2d). For high amounts (DS 20 and 25 μm) the surfaces were optically more heterogeneous and the cracking tendency increased (Figure 2c, f). Optically most homogeneous surface was achieved with the intermediate DS value of 30 μm (Figure 2b, e). The same conclusion was drawn by visual observation by the naked eye.

3.2. Topographical Characterization of the AuNP Surfaces. AFM topographic (Figure 3a) and phase (Figure 3b) images show an individual unsintered (air-dried) AuNP inkjet-dot. The outline of the dot was not easily distinguishable in the topograph because of the small AuNP film thickness

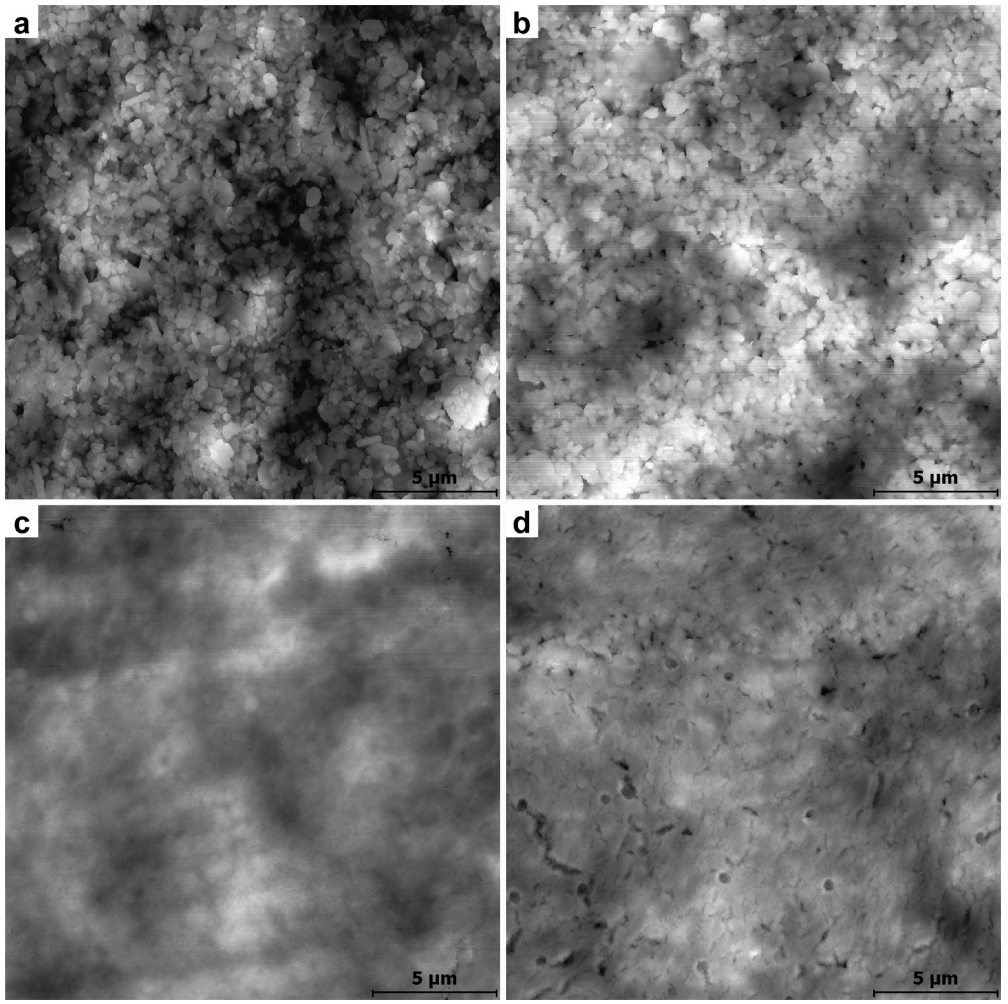

Figure 4. AFM topographical images (20 μm × 20 μm) of the (a) unprinted paper substrate and IR-sintered Au electrodes printed with DS (b) 40, (c) 30, and (d) 20 μm. The height scale is 700 nm.

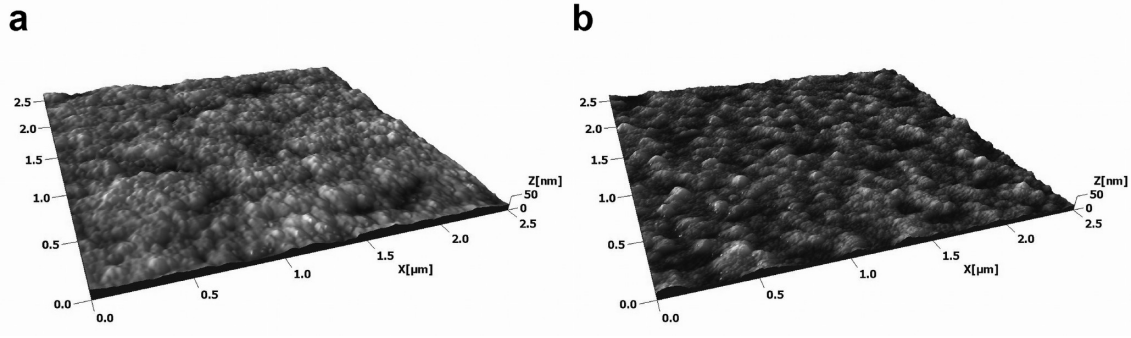

Figure 5. AFM topographical images (isometric view) of (a) an inkjet-printed and IR-sintered AuNP surface on paper (DS 30 μm) and (b) an evaporated Au surface on mica.

relative to the rough paper substrate. A sharp outline is, however, clearly distinguished in the phase image which is sensitive to differences in dissipative interactions between the tip and the sample (mainly due to variations in viscoelastic and adhesive properties of the sample).[49] The high contrast and fairly homogeneous phase angle in the dot area confirm the presence of a continuous Au layer (Figure 3b). The shape of the dot was fairly spherical with a diameter of 75 μm (Figure 3b) and a thickness of 75−100 nm (Figure 3a).

AFM topographical images show the paper substrate and the sintered AuNP films printed with different DS (Figure 4). A low amount of printed ink (DS 40 μm, 676 drops/mm^2) resulted in a relatively thin film (average thickness of 175 ± 50 nm) and the platy kaolin pigments and grain boundaries between them were still partially visible (Figure 4b). In addition, the root-mean-square (RMS) roughness of the paper substrate (96 nm) and the AuNP film (106 nm) surface was on the same range. With an intermediate ink amount (DS 30 μm, 1179 drops/mm^2), a continuous AuNP film was formed

dx.doi.org/10.1021/am201609w | ACS Appl. Mater. Interfaces 2012, 4, 955−964

(Figure 4c). The average thickness of the AuNP layer was 230 ± 60 nm (Supporting Information 3) with an RMS roughness of 57 nm. Inkjet-printing with a high ink amount (DS 20 μm, 2601 drops/mm^2) resulted in a surface with an RMS roughness of 56 nm (Figure 4d) being almost equal to that of the DS 30 μm film. However, some defects are apparent on the surface. The average thickness of the AuNP layer printed with DS 20 was 550 ± 100 nm.

A high-resolution AFM topograph shows the particulate structure of an inkjet-printed AuNP surface on paper (after IR-sintering) (Figure 5a). The Au surface was composed of homogeneously distributed nanoaggregates with an average height of around 30 nm. The RMS roughness of the image was 5 nm. This was comparable to the RMS roughness (6 nm) of an evaporated Au surface on mica (Figure 5b).

3.3. Electrical Characterization of the AuNP Structures. Electrical characterization of the printed and IR-sintered Au structures was done by measuring the resistance of a series of test lines printed with a DS value of 30 μm. The following average dimensions were determined for the Au lines: d = 224 ± 83 nm (by AFM), W = 208 ± 24 μm (by OM) and L = 2 cm. An average R of 66.7 ± 5.9 Ω was obtained, which resulted in a resistivity of 1.6 ×10^{-7} Ωm. Tolerance towards bending and twisting is shown in Supporting Information, video 1.

3.4. Contact Angle Measurements. Figure 6 shows the apparent contact angle of water ($\theta_{w,a}$) as a function of time for inkjet-printed Au surfaces with different treatments. The $\theta_{w,a}$ value of the air-dried sample was slightly above 90° and the IR-sintered sample stabilised at a level slightly below 90°. Plasma (air) cleaning decreased the $\theta_{w,a}$ value, making the surface hydrophilic. Thiolation of the AuNP surfaces by ODT turned the surface hydrophobic ($\theta_{w,a}$ > 105°). The reference substrate (evaporated Au on mica) showed hydrophilic characteristics and the measured $\theta_{w,a}$ value was close to that obtained with a similar cleaning procedure.[47] However, the relatively high $\theta_{w,a}$ value compared to a pure gold surface with zero contact angle shows that the evaporated Au surface had been readily contaminated in ambient atmosphere.[50] In all cases, the $\theta_{w,a}$ values were higher compared to that of the paper substrate (56°).

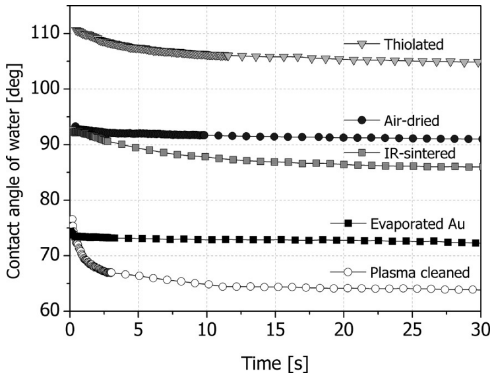

Figure 6. Apparent contact angle of water ($\theta_{w,a}$) as a function of time for inkjet-printed AuNP surfaces with different treatments. Also shown is the $\theta_{w,a}$ curve for an evaporated Au surface on mica.

3.5. Chemical Characterization by XPS. Table 1 lists the elemental composition of the inkjet-printed Au surfaces as determined from the XPS spectra. All the values are an average of three parallel measurements. In all the samples, the main component on the surface was carbon (C) and the presence of oxygen (O) was negligible (Table 1). IR-sintering decreased the C content and increased the Au and S content. Plasma cleaning had no influence on the Au content, but the S content decreased. The ODT thiolation increased the relative amount of C, whereas the relative amount of Au and S decreased.

Table 1. Binding Energies (B.E.) and Atomic Percentages (at %) of Elements for Inkjet-Printed Au Surfaces after Different Treatments

element	B.E.	air-dried (at %)	IR-sintered (at %)	plasma cleaned (at %)	thiolated (at %)
C1s	285	89.1 ± 1.7	69.1 ± 2.0	70.9 ± 0.4	80.3 ± 2.4
Au4f	85	10.0 ± 0.5	26.1 ± 1.6	26.0 ± 0.1	18.1 ± 3.5
S2p	165	0.9 ± 0.8	4.8 ± 1.2	2.8 ± 0.5	1.0 ± 0.6

High resolution spectra for the sp2 peak are shown in Figure 7. Each $S2p_{3/2}/S2p_{1/2}$ doublet was fitted by two peaks with a fixed intensity ratio of 2:1 and energy separation of 1.2 eV.[51−54] A high resolution spectrum for the air-dried sample showed the presence of two separate doublets, with main peaks at 161.5 eV (S1) and 162.9 eV (S2) (Figure 7a). After IR-sintering, three separate doublets were indentified; at 161.7 eV (S1), 163.3 eV (S2), and 168.7 eV (S3) (Figure 7b). In the plasma-cleaned sample, two doublets at 162 eV (S1) and 168.7 eV (S3) were observed (Figure 7c). After thiolation, the spectrum showed only a single doublet at 162.1 eV (Figure 7d).

3.6. Surface Potential Imaging. Figure 8 shows SP images of the inkjet-printed AuNP surfaces after different treatments. In addition, contact potential difference (CPD) histograms obtained from the respective images are depicted in Figure 9. Evaporated Au on mica substrate was used as a reference sample in all the measurements. Although the reference substrate cannot be considered to be a clean Au surface, it is assumed here that a contaminant layer will contribute equally to the CPD shifts for each sample. The CPD for clean metal surfaces is given by the difference in the work functions of the sample and reference electrode.[55] However, the work functions can be changed by adsorption of molecules with different dipole moments. Thus, in ambient conditions, the CPD is dependent not only on the material but also on the state of the surface, such as its contamination and monolayer coating.[55] Each sample showed a reasonably homogeneous SP image with no clear contrast differences resulting in a single peak in the CPD histograms. The peak position for the AuNP surfaces appeared at less negative values compared to the reference surface. The plasma cleaning of AuNP caused a positive CPD shift of 85 mV compared to the IR-sintered (uncleaned) surface. The ODT thiolation caused a further positive CPD shift of 406 mV compared with the plasma-cleaned samples.

4. DISCUSSION

4.1. Print Quality of AuNP Structures. Print quality in conventional graphical printing is often determined based on an optical response (e.g., gloss of printed film) or even a subjective visual impression.[56] However, in printed electronics, the final print quality is a measure of the electrical performance of the final components.[22] Physical properties such as surface roughness, thickness, and homogeneity of the printed layers play an important role in achieving optimal performance.[22,45]

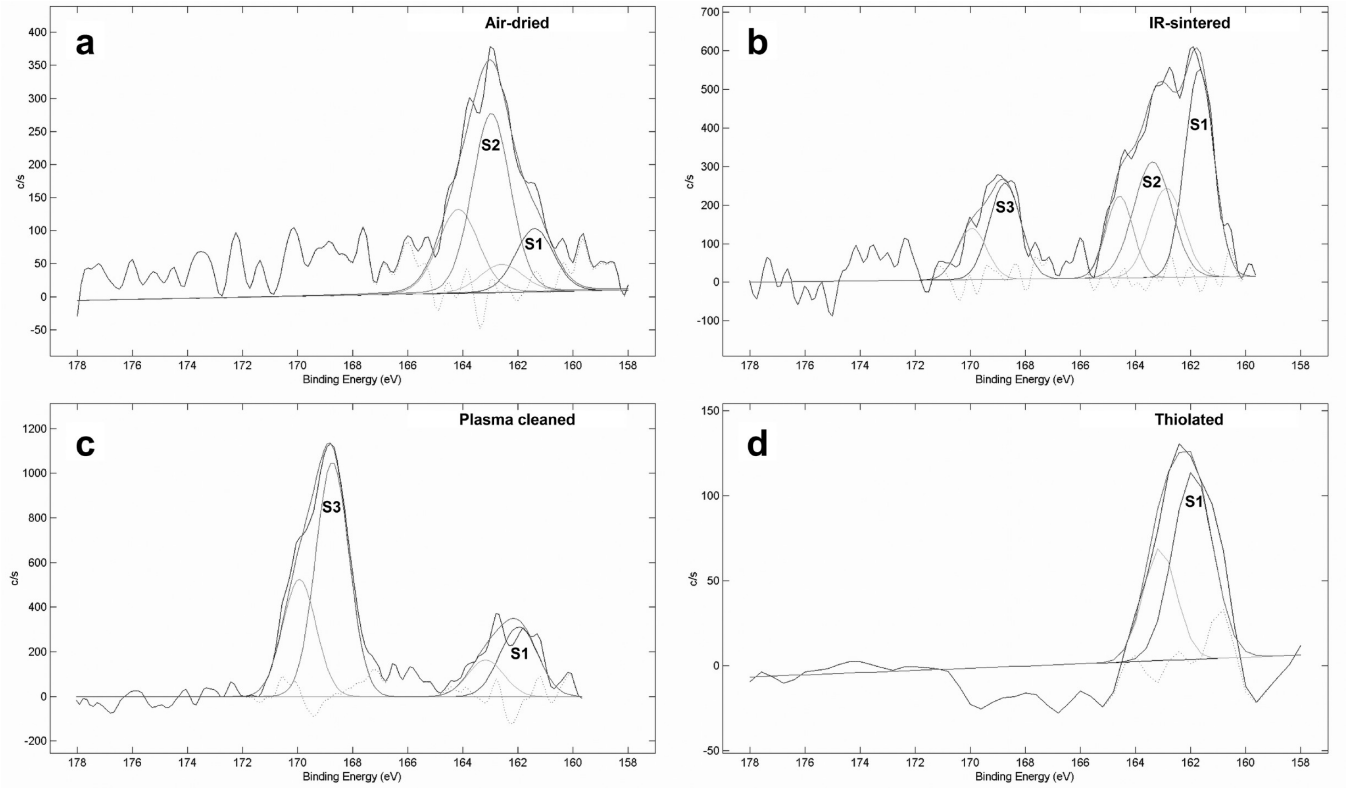

Figure 7. High-resolution XPS S2p spectra of (a) air-dried, (b) IR-sintered, (c) plasma (air)-cleaned, and (d) ODT-thiolated sample. The curve fitting of the respective S2p photopeaks are also shown.

Sublimation of the protecting agent (dodecanethiol) and subsequent coalescence of AuNPs during IR sintering is indicated by a colour change in the print (Figure 1). Coalescence of dodecanethiol-encapsulated AuNPs with size of 5 nm has been shown to occur at 170−180 °C after 30 min annealing.[12] On the other hand, the melting of AuNPs in the size range of few nanometers has been reported to occur between 300−400 °C.[37] With the current IR-sintering set-up, the paper surface is heated to about 180 °C[57] for a relatively short time (10−15 s). However, the local increase in temperature is expected to be much higher on the AuNP surface due to the lower mass per area and specific heat capacity of Au (0.126 J g^{-1} K^{-1})[58] compared to paper substrate (0.134 J g^{-1} K^{-1}).[59] Topographical analysis shows that after IR-sintering the gold surface is composed of larger aggregates (~30 nm, Figure 5a) compared to the average size of AuNPs in the ink (~3 nm, Supporting information 1). This supports the sintering-induced coalescence of particles.

AFM analysis shows that a very small amount of AuNP ink ($V \approx 10$ pL) is sufficient to form a continuous gold layer on the paper surface (Figure 3). This serves as a demonstration of the nearly plastic like barrier properties against liquid penetration of the proprietary paper substrate. The diameter of the circular print area (compared to its pendant droplet diameter) is consistent with that shown previously for the spreading of low-surface tension and low-viscosity inks on similar pigment-coated paper substrates.[45] The diameter of the spread droplet is affected by the surface energy and porosity of the substrate as well as the properties of the ink (surface tension, density, viscosity) and the inkjet-printing itself (inertia due to the droplet impact). A common problem in inkjet-printing with low-viscous and low-surface tension inks is the accumulation of solid material in the perimeter of the droplet during the evaporation of the solvent (i.e. the coffee-ring phenomenon).[60,61] The final drying pattern of a concentrated suspension in the form of a sessile drop is influenced by the lateral flow needed to compensate for evaporative losses from the droplet periphery.[60,61] This is considered as the main cause of the coffee-ring effect. In addition, the final patterns are affected by the Marangoni flow by inducing circulatory flows in the drying droplet and the sedimentation due to gravitational force.[62,63] No coffee-ring phenomenon was observed when AuNP-ink droplets were inkjet-printed on the paper substrate (Figure 3). The partial absorption of liquid into the porous paper compensates for the evaporation of the solvent and reduces the effect of lateral flow on the material distribution. Thus, a homogeneous material distribution was achieved.

A sufficient density of the AuNP material is needed for the heat-induced sintering to occur leading in the formation of conductive structures (Figures 1 and 2). Low resistance AuNP films were achieved even with a DS value of 40−45 μm. However, with such a low amount of ink and a small layer thickness (Figures 4b), the edges of the printed structures were less dense and were not properly sintered (Figure 2a). During levelling and consolidation, particulate coating materials have a tendency to accumulate towards the cavities and pores.[64] This is supported by the decrease in Sq with increased ink amount.

Too high an amount of the dispensed ink leads to both an optically (Figure 2c) and microscopically (Figure 4d) heterogeneous surface including defects. Formation of defects during annealing has been observed for thick NP films experiencing a large volume reduction.[65,66] For the inkjet-printed AuNP structures studied here, a volume reduction of over 50% per area after IR-sintering was established

dx.doi.org/10.1021/am201609w | ACS Appl. Mater. Interfaces 2012, 4, 955−964

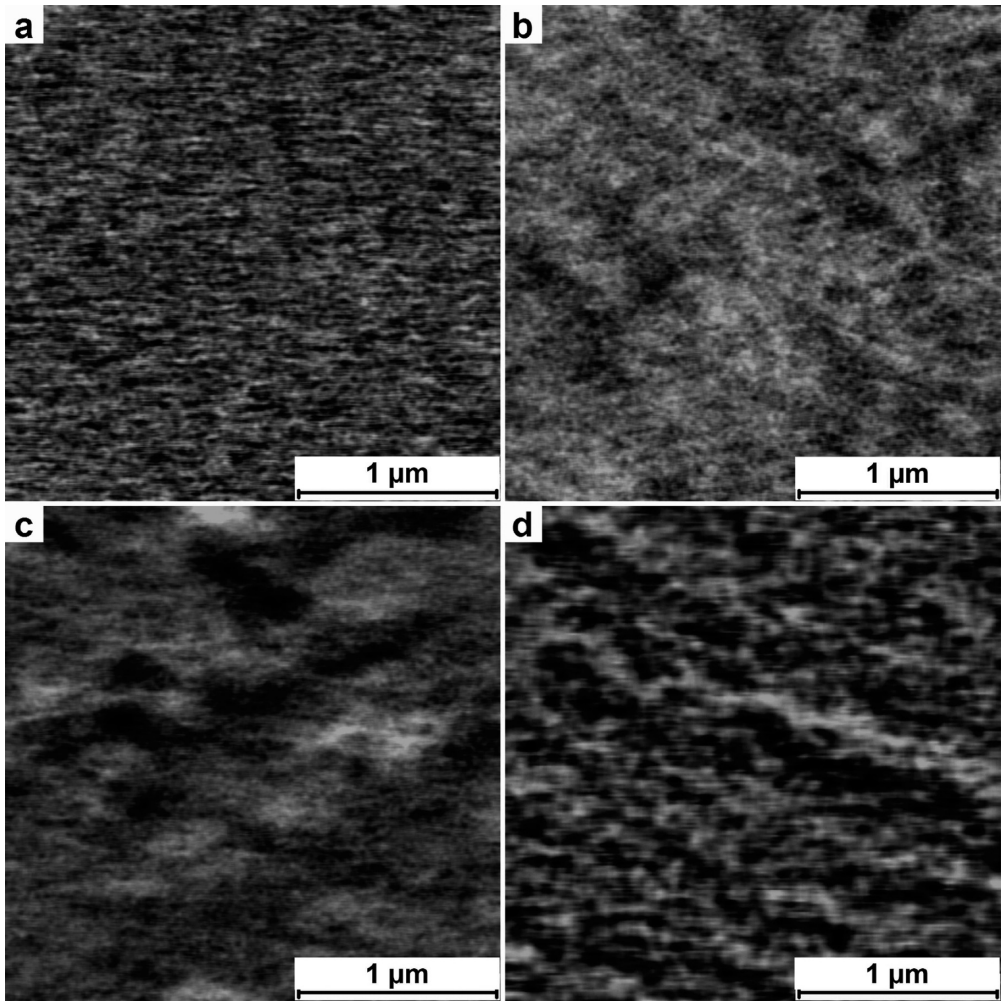

Figure 8. Surface potential images for (a) evaporated Au surface on Mica, (b) IR-sintered AuNP surface, (c) plasma-cleaned AuNP surface, and (d) ODT-thiolated AuNP surface. The image size is 2.5 μm × 2.5 μm and the colour contrast is (a) 75, (b) 100, (c) 150, and (d) 60 mV.

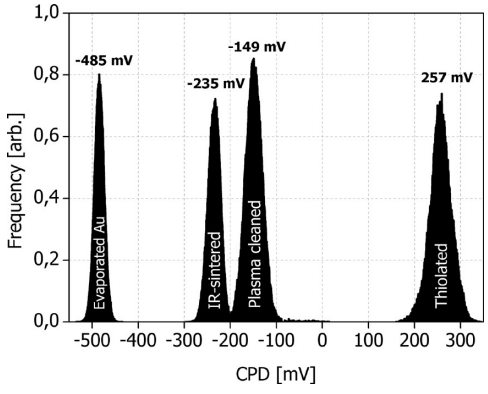

Figure 9. Contact potential difference (CPD) histograms for the studied samples.

(Supporting Information 4). In addition, pre-existing cracks, heterogeneous stress distribution, hindered evaporation of solvent, poor adhesion and different thermal expansion coefficients of the film and the substrate contribute to the formation of defects.[19,65−69]

Optically and microscopically the most homogeneous sintered AuNP film (Figure 2b) with a resistivity (ρ) of 1.6 $\times 10^{-7}$ Ω m was achieved using a DS value of 30 μm. Obviously, this ink amount was large enough for enabling a successful IR-sintering process which involves rapid solvent evaporation and a relatively large volume reduction. Although the resistivity value was about one order of magnitude above the resistivity of bulk gold, it is in agreement with the values that have been reported previously for inkjet-printed AuNP tracks on a glass substrate.[42] This indicates that the used paper substrate was smooth enough not to have a significant adverse effect on the conductivity of the AuNP structures. Porosity in the inkjet-printed Au film has been regarded as the main reason for the achieved lower conductivities compared to bulk gold.[40]

Performance of the inkjet-printed AuNP electrodes on paper was tested further in an aqueous electrolyte medium. A configuration of gold electrodes (Figure 10 a) consisting of two hemi-circular electrodes (separated by 300 μm) and two gold wires (15 mm × 1 mm) as contacts were used. A drop (20 μL) of electrolyte HEPES-EDTA buffer solution was pipetted on the electrode area and the resistance of the thereby closed circuit was measured (Figure 10 b). A hydrophobic and transparent polydimethylsiloxane (PDMS) based ink layer was inkjet-printed around the perimeter of the electrodes to confine the electrolyte drop in the correct place (Figure 10a).[70] The excellent barrier properties of the coated paper substrate prevented the absorption of the liquid inside the paper. A closed circuit became apparent through a measurable resistance immediately after a drop of buffer solution was introduced and

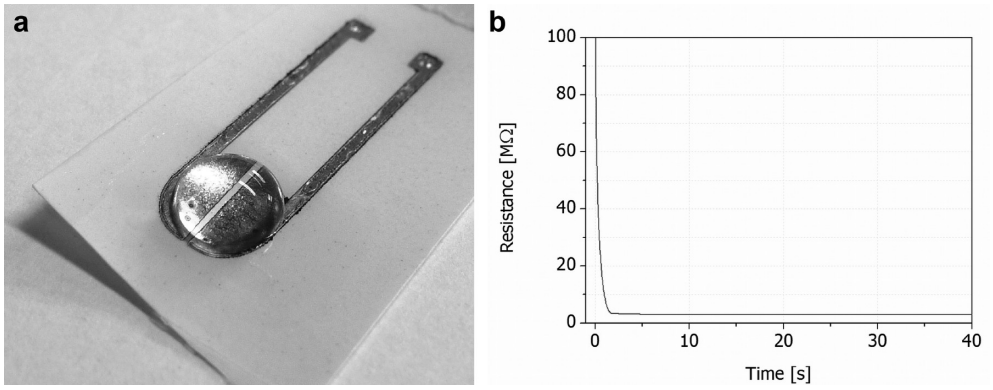

Figure 10. (a) Photograph of the AuNP electrode structure with electrolyte buffer dispensed over the electrode area. (b) Resistance between the printed electrodes as a function of time after the application of HEPES-EDTA buffer (pH 7.4) solution.

the resistance stabilised finally around 2.9 MΩ (Figure 10b). This demonstrates the possibility of using printed gold electrodes in paper-based electrochemical applications.[71]

4.2. Surface Chemistry and Functionalization of AuNP Structures. The S2p spectrum of the air-dried sample is in accordance with the XPS results shown for amorphous gold sulfide (Au_2S) nanoparticles (Figure 7a).[72] This suggests that the majority of the protecting agents (dodecanethiols) are chemisorbed to AuNPs via an AuS(R)Au bond (S2, Figure 7a) and only the minority (~20%) via gold thiolate (Au-SR) bond (S1, Figure 7a).

The presence of carbon and sulfur species on the surface shows that the removal of the stabilising thiol by IR-sintering is not complete (Table 1). The doublet at 161.7 eV in the Sp2 core spectra (Figure 7b) indicates that part of the sulfur species is still bound to the AuNPs via an Au-SR bond.[53,54] The S2 doublet is slightly shifted to a higher binding energy (from 162.9 eV to 163.3 eV) and the intensity ratio of S1 and S2 is clearly changed (Figure 7a and 7b). This indicates the decomposition of AuS(R)Au bonds by IR irradiation and the formation of Au-SR and unbound thiols (RSH or RSSR).[51,53] The decomposition and oxidation of unbound thiols to sulfates (RSO_x) is confirmed by the presence of the peak at 168.7 (S3) (Figure 7b).[51,53] A change in the water wetting properties of the AuNP surface further confirms the IR irradiation induced removal and oxidation of the stabilising agents (Figure 6). In addition, the presence of IR-sintering residues on AuNP surface leads both to an approximate 13° higher $\theta_{w,a}$ value (Figure 6) and a positive CPD shift (250 mV) compared to evaporated Au surface on mica (Figure 9). The difference in $\theta_{w,a}$ values must come solely from the difference in surface chemistry as the roughness was very similar between the samples (Figure 5).

The lack of unbound sulfur doublet (S2) and a significant increase in intensity of oxidised sulfur peak (S3) relative to bound thiol doublet show that majority of sulfur species are oxidised by plasma treatment (Figure 7c). Clearly the hydrophilic surface further confirms the change in chemistry (Figure 6). Mild O_2 plasma and UV/ozone treatments have been shown to remove contaminants and thiol SAMs from metal surfaces.[47,73] This is indicated by a decreased intensity of the S1 peak (Figure 7b and 7c). The aforementioned changes in surface chemistry lead to a positive shift of 86 mV in CPD (Figure 9).

The plasma-cleaned AuNP surface turned hydrophobic after thiolation (Figure 6). It has been established previously that long-chain alkanethiols form a well-packed, pseudocrystalline, oriented monolayer on gold in which the hydrocarbon chains are in all-trans conformation and tilted ~30° from the normal of the surface.[74−76] The $\theta_{w,a}$ value is quite close to that previously observed for ODT SAMs on Au ($\theta_{w,a}$ ~110°).[77] XPS results show that the C/Au ratio increased considerably after thiolation, indicating an increased thickness in the organic layer on AuNP surface (Table 1). Furthermore, high-resolution spectrum of Sp2 shows only one doublet at 162.1 eV, indicating that the ODT molecules are bound to the AuNP surface solely via thiolate bonds (Figure 7d).[53,54] Using the intensities of C and Au peaks, and the attenuation length of 4.2 nm for C1s photoelectrons in hydrocarbon film, the thickness of the ODT monolayer was estimated using the instrument's software to be 2.0 ± 0.4 nm.[78,79] The thickness value is in accordance with the expected thickness (~2.0−2.4 nm) for a fully orientated ODT SAM on Au.[77] Compared to the plasma cleaned surface, the CPD value of the thiolated sample shifted +406 mV (Figure 9). Alkanethiol monolayers adsorbed onto an Au surface may be considered as a two-dimensional assembly of dipoles with a layer of negative charges residing close to the Au-monolayer interface and a layer of positive charges residing closer to the monolayer−air interface.[80] This induces a shift towards positive surface potential values compared to the bare Au reference.[55,80−86] The magnitude of the shift is dependent upon the length of the alkyl chain (9.9−20 mV per CH_2 unit), orientation of the dipoles, and surface coverage of the monolayer. The measured CPD shift (+406 mV) after thiolation is in accordance with the value obtained for a fully orientated alkanethiol film.[81,83] The above results confirm the successful functionalisation of the plasma-cleaned AuNP surface with an ODT SAM.

5. CONCLUSIONS

This paper demonstrates the fabrication functionalization of conductive Au patterns on recyclable paper by an inkjet-printing process. The conductivity of the electrodes after low temperature IR-sintering was comparable with the previously reported values obtained for printed Au electrodes on glass substrates. This shows that the substrate roughness or the organic residues remaining after the IR-sintering do not have a significant effect on the resistance of the printed Au films. The use of a flexible paper substrate and roll-to-roll compatible printing technique together with rapid sintering enable the mass-manufacturing of Au electrodes for high-volume and large area applications. In addition, successful formation of high quality SAMs on the printed Au films will create a wide range of

possibilities in applications involving molecular recognition, e.g., in printed diagnostics. This will be addressed in future studies.

■ ASSOCIATED CONTENT

Supporting Information

A TEM image of the synthesized AuNPs, a TGA curve showing the degredation of the dodecanethiol layer of the AuNPs, an AFM topographical image of the AuNP film with a corresponding height distribution histogram, AFM topographical images of the AuNP film captured exactly at the same spot before and after IR-sintering, and a video showing that the electrodes remain conductive during bending and twisting. This material is available free of charge via the Internet at http://pubs.acs.org.

■ AUTHOR INFORMATION

Corresponding Author

*Tel.: +358 2 215 4614. Fax: +358 2 233 0228. E-mail: anni.maattanen@abo.fi.

■ ACKNOWLEDGMENTS

R. Bollström is acknowledged for fabricating the paper substrate.[46] Financial support is acknowledged from the Academy of Finland through the National Center of Excellence program.

■ REFERENCES

(1) Kamyshny, A. *Open Appl. Phys. J.* **2011**, *4*, 19−36.
(2) Bidoki, S. M.; Lewis, D. M.; Clark, M.; Vakorov, A.; Millner, P. A.; McGorman, D. *J. Micromech. Microeng.* **2007**, *17*, 967−974.
(3) Perelaer, J.; smith, P. J.; Mager, D.; Soltman, D.; Volkman, S. K.; Subramanian, V.; Korvink, J. G.; Schubert, U. S. *J. Mater. Chem.* **2010**, *20*, 8446−8453.
(4) Lee, H.-H.; Chou, K.-S.; Huang, K.-C. *Nanotechnology* **2005**, *16*, 2436−2441.
(5) Ko, S. H.; Pan, H.; Grigoropoulos, C. P.; Luscombe, C. K.; Fréchet, J. M. J.; Poulikakos, D. *Nanotechnology* **2007**, *18*, 345202.
(6) Redinger, D.; Molesa, S.; Shong, Y.; Farschi, R.; Subramanian, V. *IEEE Trans. Electron. Devices* **2004**, *51*, 1978−1983.
(7) Kamyshny, A.; Ben-Moshe, M.; Aviezer, S.; Magdassi, S. *Macromol. Rapid Commun.* **2005**, *26*, 281−288.
(8) Fuller, S. B.; Wilhelm, E. J.; Jacobson, J. M. *J. Microelectromech. Syst.* **2002**, *11*, 54−60.
(9) Chrisey, D. B. *Science* **2000**, *289*, 879−881.
(10) Mo, L.; Liu, D.; Zhou, X.; Li, L. *Proceedings of the 2nd International Congress on Image and Signal Processing (CISP)*; Tianjin, China, Oct. 17−19, 2009 ; IEEE: Piscataway, NJ, 2009; pp 1−5.
(11) Calvert, P. *Chem. Mater.* **2001**, *13*, 3299−3305.
(12) Huang, D.; Liao, F.; Molesa, S.; Redinger, D.; Subramanian, V. *J. Electrochem. Soc.* **2003**, *150*, G412−G417.
(13) Jang, S.; Seo, Y.; Choi, J.; Kim, T.; Cho, J.; Kim, S.; Kim, D. *Scr. Mater.* **2010**, *62*, 258−261.
(14) Kim, J.; Cho, J.; Chung, S.; Kwak, J.; Lee, C.; Hong, Y.; Kim, J.-J. *J. Korean Phys. Soc.* **2009**, *54*, 518−522.
(15) Allen, M. L.; Aronniemi, M.; Mattila, T.; Alastalo, A.; Ojanperä, K.; Suhonen, M.; Seppä, H. *Nanotechnology* **2008**, *19*, 175201.
(16) Gizachew, Y. T.; Escoubas, L.; Simon, J.J.; Pasquinelli, M.; Loiret, J.; Leguen, P.Y.; Jimeno, J.C.; Martin, J.; Apraiz, a.; Aguerre, J.P. *Sol. Energy Mater. Sol. Cells* **2011**, *95*, 70−82.
(17) Kim, D.; Jeong, S.; Park, B. K.; Moon. *J. Appl. Phys. Lett.* **2006**, *89*, 264101.
(18) Kim, D.; Moon, J. *Electrochem. Solid-State Lett.* **2005**, *8*, J30−J33.
(19) Maekawa, K.; Yamasaki, K.; Niizeki, T.; Mita, M.; Matsuba, Y.; Terada, N.; Saito, H. *Mater. Sci. Forum* **2010**, *638−642*, 2085−2090.
(20) Shin, K.-Y.; Lee, S.-H.; Oh, J. H. *J. Micromech. Microeng.* **2011**, *21*, 045012.
(21) Bollström, R.; Määttänen, A.; Tobjörk, D.; Ihalainen, P.; Kaihovirta, N.; Österbacka, R.; Peltonen, J.; Toivakka, M. *Org. Electron.* **2009**, *10*, 1020−1023.
(22) Tobjörk, D; Österbacka, R. *Adv. Mater.* **2011**, *23*, 1935−1961.
(23) Krebs, F. C. *Org. Electron.* **2009**, *10*, 761−768.
(24) Krebs, F.C.; Norrman, K. *ACS Appl. Mater. Interfaces* **2010**, *2*, 877−887.
(25) Kim, J. B.; Kim, C. S.; Kim, Y. S.; Loo, Y.-L. *Appl. Phys. Lett.* **2009**, *95*, 183301.
(26) Wu, Y.; Li, Y.; Ong, B. S.; Liu, P.; Gardner, S.; Chiang, B. *Adv. Mater.* **2005**, *17*, 184−187.
(27) Bishop, P. T.; Ashfield, L.J.; Berzins, A.; Boardman, A.; Buche, V.; Cookson, J.; Gordon, R.J.; Salcianu, C.; Sutton, P.A. *Gold Bull.* **2010**, *43*, 181−188.
(28) Shukla, R.; Bansal, V.; Chaudhary, M.; Basu, A.; Bhonde, R. R.; Sastry, M. *Langmuir* **2005**, *21*, 10644−10654.
(29) Love, J. C.; Estroff, L. A.; Kriebel, J. K.; Nuzzo, R. G.; Whitesides, G. M. *Chem. Rev.* **2005**, *105*, 1103−1169.
(30) Skrabalak, S. E.; Au, L.; Lu, X.; Li, X.; Xia, Y. *Nanomedicine* **2007**, *2*, 657−668.
(31) Arvizo, R.; Bhattacharya, R.; Mukherjee, P. *Exp. Opin. Drug Delivery* **2010**, *7*, 753−763.
(32) Kannan, R.; Katti, K. V. In *Biomedical Applications of Nanotechnology*; Labhasetwar, V, Leslie-Pelecky, D. L., Eds.; John Wiley & Sons: Hoboken, NJ, 2007; p 173−189.
(33) Ford, M.; Masens, C.; Cortie, M. *Surf. Rev. Lett.* **2006**, *13*, 297−307.
(34) Hostetler, M. J.; Wingate, J. E.; Zhong, C.-J.; Harris, J.E.; Vachet, R.W.; Clark, M.R.; Londono, J.D.; Green, S.J.; Stokes, J.J.; Wignall, G.D.; Glish, G.L.; Porter, M.D.; Evans, N.D.; Murray, R.W. *Langmuir* **1998**, *14*, 17−30.
(35) Brust, M.; Walker, M.; Bethell, D.; Schiffrin, D.J.; Whyman, R. *J. Chem. Soc. Chem. Commun.* **1994**, *7*, 801−802.
(36) Zheng, N.; Fan, J.; Stucky, G.D. *J. Am. Chem. Soc.* **2006**, *128*, 6550−6551.
(37) Buffat, P.; Borel, J.-P. *Phys. Rev. A* **1976**, *13*, 2287−2298.
(38) Bieri, N.; Chung, J.; Poulikakos, D. *Superlatt. Microstruct.* **2004**, *35*, 437−444.
(39) Bieri, N. R.; Chung, J.; Haferl, S. E.; Poulikakos, D.; Grigoropoulos, C. P. *Appl. Phys. Lett.* **2003**, *82*, 3529−3531.
(40) Nur, H. M.; Song, J. H.; Evans, J. R. G.; Edirisinghe, M. J. *J. Mater. Sci.: Mater. Electron.* **2002**, *13*, 213−219.
(41) Chung, J.; Ko, S.; Bieri, N. R.; Grigoropoulos, C. P.; Poulikakos, D. *Appl. Phys. Lett.* **2004**, *84*, 801−803.
(42) Samarasinghe, S.R.; Pastoriza-Santos, I.; Edirisinghe, M.; Reece, M.; Liz-Marzin, L.; Nangrejo, R.; Ahmad, Z. *Nat. Sci.* **2009**, *1*, 142−150.
(43) Jensen, G. C.; Krause, C. E.; Sotzing, G. A.; Rusling, J. F. *Phys. Chem. Chem. Phys.* **2011**, *13*, 4888.
(44) Tobjörk, D.; Aarnio, H.; Pulkkinen, P.; Bollström, R.; Määttänen, A.; Ihalainen, P.; Mäkelä, T.; Peltonen, J.; Toivakka, M.; Tehnu, H.; Österbacka, R. *Thin Solid Films* **2011**, DOI: 10.1016/j.tsf.2011.10.017.
(45) Määttänen, A.; Ihalainen, P.; Bollström, R.; Toivakka, M.; Peltonen, J. *Colloids Surf., A* **2010**, *367*, 76−84.
(46) Bollström, R.; Määttänen, A.; Ihalainen, P.; Peltonen, J.; Toivakka, M. Method for creating a substrate for printed or coated functionality, substrate, functional device and its use. PCT/FI2010/050056, WO 2010/086511.
(47) Ron, H.; Matlis, S.; Rubinstein, I. *Langmuir* **1998**, *14*, 1116−1121.
(48) Ferry, F.M.; Kjoller, K.; Thornton, J.T.; Tench, R.J.; Cook, D. *Electrical Force Microcopy, Surface Potential Imaging and Surface Electric Modification with the Atomic Force Microcope (AFM), Application Notes 27*; Bruker AXS: Madison, WI.
(49) García, R.; Pérez, R. *Surf. Sci. Rep.* **2002**, *47*, 197−301.
(50) Bewig, K.W.; Zisman, W.A. *J. Phys. Chem.* **1965**, *69*, 4238−4242.

(51) Dietrich, P. M.; Horlacher, T.; Girard-Lauriault, P.-L.; Gross, T.; Lippitz, A.; Min, H.; Wirth, T.; Castelli, R.; Seeberger, P.H.; Unger, W.E.S. *Langmuir* **2011**, *27*, 4808−4815.
(52) Abdureyim, A.; Okudaira, K.K.; Harada, Y.; Masuda, S.; Aoki, M.; Seki, K.; Ito, E.; Ueno, N. *J. Electron. Spectrosc. Relat. Phenom.* **2001**, *114*−*116*, 371−374.
(53) Zharnikov, M.; Frey, S.; Heister, K.; Grunze, M. *Langmuir* **2000**, *16*, 2697−2705.
(54) Castner, D. G.; Hinds, K.; Grainger, D. W. *Langmuir* **1996**, *12*, 5083−5086.
(55) Lü, J.; Delamarche, E.; Eng, L.; Bennewitz, R.; Meyer, E.; Güntherodt, H. *Langmuir* **1999**, *15*, 8184−8188.
(56) Kipphan, H. *Handbook of Print Media*; Springer: Berlin, 2001; p 68.
(57) Saarinen, J.J; Ihalainen, P.; Määttänen, A.; Bollström, R.; Peltonen, J. *NSTI-Nanotechnol.* **2010**, *2*, 527−530.
(58) Tipler, P. A. *Physics for Scientists and Engineers*, 4th ed.; W.H. Freeman: New York, 1999.
(59) The Engineering ToolBox home page: Solids − Specific Heats http://www.engineeringtoolbox.com/specific-heat-solids-d_154.html (accessed Oct 14, 2011).
(60) Deegan, R. D.; Bakajin, O.; Dupont, T. F.; Huber, G. S.; Nagel, R.; Witten, T. A. *Nature* **1997**, *389*, 827−829.
(61) Deegan, R. D.; Bakajin, O.; Dupont, T. F.; Huber, G.; Nagel, S. R.; Witten, T. A. *Phys. Rev. E* **2000**, *62*, 756.
(62) Yiantsios, S. G.; Higgins, B. G. *Phys. Fluids* **2006**, *18*, 082103.
(63) Hu, H.; Larson, R. G. *J. Phys. Chem. B* **2006**, *110*, 7090−7094.
(64) Dahlström, C.; Uesaka, T. *Ind. Eng. Chem. Res* **2009**, *48*, 10472−10478.
(65) Kang, J. S.; Kim, H. S.; Ryu, J.; Hahn, H. T.; Jang, S.; Joung, J. W. *J. Mater. Sci.: Mater. Electron.* **2010**, *21*, 1213−1220.
(66) Greer, J. R.; Street, R. A. *J. Appl. Phys.* **2007**, *101*, 103529.
(67) Sivaramakrishnan, S.; Chia, P.-J.; Yeo, Y.-C.; Chua, L.-L.; Ho, P. K.-H. *Nat Mater* **2007**, *6*, 149−155.
(68) Jung, J.-K.; Choi, S.-H.; Kim, I.; Jung, H. C.; Joung, J.; Joo, Y.-C. *Philos. Mag.* **2008**, *88*, 339−359.
(69) Lee, D. J.; Oh, J. H.; Bae, H. S. *Mater. Lett.* **2010**, *64*, 1069−1072.
(70) Määttänen, A.; Fors, D.; Wang, S.; Valtakari, D.; Ihalainen, P.; Peltonen, J. *Sens. Actuators, B* **2011**, *160*, 1404−1412.
(71) Ihalainen, P.; Määttänen, A.; Mattinen, U.; Stępień, M.; Bollström, R.; Toivakka, M.; Bobacka, J.; Peltonen, J. *Thin Solid Films* **2011**, *519*, 2172−2175.
(72) Mikhlin, Y.; Likhatski, M.; Tomashevich, Y.; Romanchenko, A.; Erenburg, S.; Trubina, S. *J. Electron. Spectrosc. Relat. Phenom.* **2010**, *177*, 24−29.
(73) Ron, H.; Rubinstein, I. *Langmuir* **1994**, *10*, 4566−4573.
(74) Nuzzo, R. G.; Allara, D. L. *J. Am. Chem. Soc.* **1983**, *105*, 4481−4483.
(75) Porter, M. D.; Bright, T. B.; Allara, D. L.; Chidsey, C. E. D. *J. Am. Chem. Soc.* **1987**, *109*, 3559−3568.
(76) Bain, C. D.; Whitesides, G. M. *J. Am. Chem. Soc.* **1989**, *111*, 7164−7175.
(77) Biebuyck, H. A.; Bain, C. D.; Whitesides, G. M. *Langmuir* **1994**, *10*, 1825−1831.
(78) Bain, C.; Whitesides, G. M. *J. Phys. Chem.* **1989**, *93*, 1670−1673.
(79) Laibinis, P. E.; Bain, C. D.; Whitesides, G. M. *J. Phys. Chem.* **1991**, *95*, 7017−7021.
(80) Evans, S. D.; Ulman, A. *Chem. Phys. Lett.* **1990**, *170*, 462−466.
(81) Alloway, D. M.; Hofmann, M.; Smith, D. L.; Gruhn, N. E.; Graham, A. L.; Colorado, R.; Wysocki, V. H.; Lee, T. R.; Lee, P. A.; Armstrong, N. R. *J. Phys. Chem. B* **2003**, *107*, 11690−11699.
(82) Ratner, M. *Nature* **2000**, *404*, 137−138.
(83) Alloway, D.M.; Graham, A.L.; Yang, X.; Mudalige, A.; Colorado, R. Jr.; Wysocki, V.H.; Pemberton, J.E.; Lee, T.R.; Wysocki, R.J.; Armstrong, N.R. *J. Phys. Chem. C* **2009**, *113*, 20328−20334.
(84) Ratner, M. *Nature* **2005**, *435*, 575−577.
(85) Saito, N.; Hayashi, K.; Sugimura, H.; Takai, O.; Nakagiri, N. *Surf. Interface Anal.* **2002**, *34*, 601−605.
(86) Stroeve, P. In *Encyclopedia of Nanoscience and Nanotechnology*, 2nd ed.; Contescu, C., Putyera, K., Eds., CRC Press: Boca Raton, FL, 2008; p 3738.